Raja Sekhar Dondapati*1*

Investigations on Forced Flow Cooling Strategy for Solenoid Superconducting Magnetic Energy Storage (SMES) Devices Using High Temperature Superconducting (HTS) Cables Cooled by Supercritical Nitrogen (SCN)



Abstract

Superconducting Magnetic Energy Storage (SMES) devices are the most reliable and promising in terms of energy density and energy security. However, the challenges encountered by these devices can be overcome by adapting suitable cooling strategies. Instead of using superconducting tapes on the Mandrel, High Temperature Superconducting (HTS) power cables can be wound on the mandrel due to higher energy density and due to higher energy storage capacity. While operating, SMES encounter few losses such as Alternating Current (A.C) losses in the superconducting tapes, dielectric losses in the dielectric material and thermal losses in the cryostat. The HTS cables wound on the mandrel mainly comprise of conductor phase consisting of HTS tapes enveloped in cryostat (two concentric corrugated pipes). The inner corrugated pipe is used as former in which the coolant flows to maintain the superconductivity of HTS tapes. The outer corrugated pipe of cryostat is wrapped with XLPE (Cross-Linked Poly Ethelene) to prevent the heat-in-leaks from the ambient. The thermal losses in HTS cables are mainly due to axial heat-in-leak from current leads, radial heat leak through insulating materials, cryostat-pipes and heat generation in the superconducting tapes. It is therefore necessary to investigate the effect of different heat flux on pressure drop and heat transfer. In the present work, an attempt has been made to propose Supercritical Nitrogen (SCN) as an alternative coolant for futuristic high temperature superconductors such as Hg (Mercury) based HTS tapes having critical temperature greater than 134K. Moreover, the effect of various heat fluxes and mass flow rates on pressure drop and heat transfer phenomenon in the futuristic SMES is also investigated using Computational Fluid Dynamics (CFD) algorithm. Finally, the pressure drop and heat transfer results of SCN are then compared with those of Liquid Nitrogen (LN2) experimental and computational results available in the literature.

Keywords: Superconducting Magnetic Energy Storage; HTS Cables; Supercritical Nitrogen; Room temperature Superconductors; friction factors; Heat transfer;

INTRODUCTION

Superconducting Magnetic Energy Storage (SMES) devices are advanced energy storage systems that utilize the unique properties of superconductors to efficiently store and release electrical energy. These systems are capable of storing energy for prolonged periods with minimal losses [1] and can provide fast and reliable responses to fluctuations in the electrical grid. SMES devices are particularly valuable in applications where rapid and high-power energy injection or absorption is required [2]. Despite their advantages, SMES devices also have some limitations. One significant challenge is the need for cryogenic cooling [3] to maintain the superconducting state, which can lead to higher operational costs. Additionally, the development of suitable superconducting materials that can operate at higher temperatures and in practical conditions is an ongoing area of research. While they present challenges, they hold the potential to enhance grid stability and support the transition towards a more sustainable energy future. In the recent past, it is suggested coolants such as Liquid Nitrogen (LN₂) [4], Super Critical Nitrogen (SCN) [5], Supercritical Argon (SCAR) [6] for efficient working. However, these cooling techniques are not found to be excessively beneficial. Hence, requirement of a novel cooling strategies for Superconducting Magnetic Energy Storage (SMES) are required to be developed. In order to increase the current density and to enhance the cooling of SMES, Forced flow of Supercritical Nitrogen (SCN), a High Temperature Superconducting (HTS) cable can be wound around the Mandrel of solenoidal SMES as shown in Figure 1. The utility of mixed cryogenic fluid can be another alternative cooling solution for HTS cables [10]. Further, HTS power cables that are cooled by forced circulation of liquid nitrogen in sub cooled state to reduce heat loss and maintain cryogenic environment is investigated [11]. In addition, the flow characteristic of pressure drop of LN2 in long length HTS cable and heat transfer, AC loss, heat leak in cryostat-pipes [12] was investigated. Later, a new concept of integrating refrigerator for cryogenic cooling in long-length of HTS cables with liquid nitrogen circulation to eliminate the cryogenic pumps was proposed [13].

^{*}School of Mechanical Engineering, Lovely Professional University, Phagwara, Punjab 144411, India. drsekhar@ieee.org



Figure 1 High Temperature Superconducting (HTS) cable wound around the Mandrel of Solenoid type Superconducting Magnetic Energy Storage (SMES)

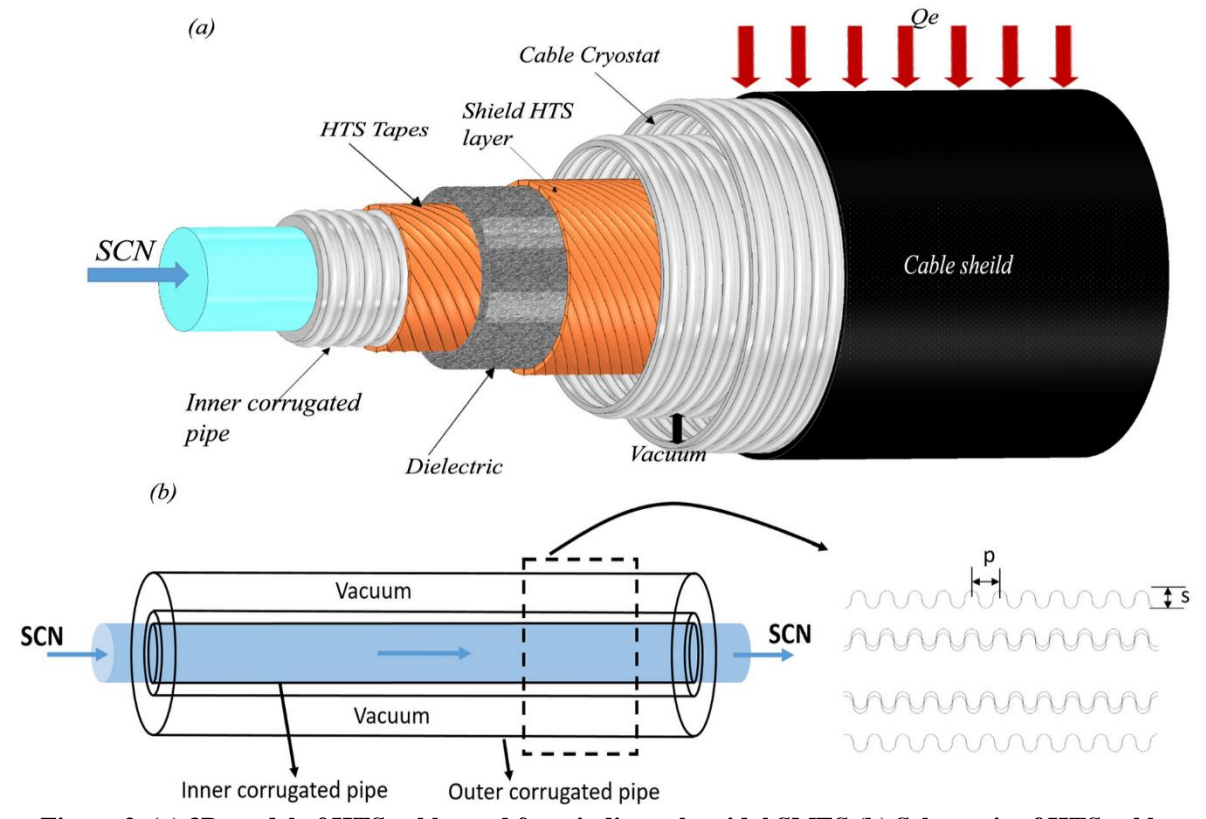


Figure 2. (a) 3D model of HTS cable used for winding solenoidal SMES (b) Schematic of HTS cable

PROBLEM DESCRIPTION

In this work, the effect of heat flux from different sources such as AC losses through HTS conductor, axial heat conduction from current leads, dielectric losses from dielectric material and radial heat in leaks from ambient are considered to estimate their effect on pressure drop and heat transfer in corrugated pipe (former) as shown in Figure 2(b). The geometrical parameters of HTS cable such as corrugation pitch and diameter of domain are 6 mm and 40 mm

respectively. However, for the present analysis, governing equations are solved for steady state, incompressible and turbulent flow of supercritical nitrogen (SCN) through corrugated steel pipe. In order to represent the actual superconducting transmission system, the dimensional parameters for the present work are considered constant with varying volumetric flow rates from 10 L/min to 30 L/min and total heat load including AC losses, dielectric losses and heat-in-leak from 1 W/m to 5 W/m are considered. The thermo-physical properties of the supercritical nitrogen used as coolant in the present analysis are shown in Table 1. Further, the electrical parameters considered for the present analysis is shown in Table 2.

Table 1 Thermophysical properties of SCN and LN2 [14]

Cryogen	State	Temperature (K)	Pressure (bar)	Density (kg/m³)	Cp (kJ/kg-K)	Thermal Conductivity (W/m-K)	Viscosity (Pa-s)
SCN	Supercritical	126.19	33.958	342.67	729.99	0.13472	2.0645 x10 ⁻⁵
LN2	Sub cooled	65	Average of (1-10)	860.554	1.998	0.173612	0.000282

Table 2 Electrical and therm	nal parameters of HTS tapes
------------------------------	-----------------------------

Tubic 2 Electrical and thermal parameters of 1115 tapes								
Amperage (Amps)	AC Loss (W/m)	Total AC loss (W)	Heat Flux (W/m2)					
250	0.016082305	0.07587149	33519.54484					
275	0.021405548	0.100984953	44614.51419					
300	0.027790223	0.131105934	57921.77349					

1. SOLUTION METHODOLOGY

The computational method is adapted to investigate the effect of heat flux on pressure drop and heat transfer in HTS cable which includes modelling a computational flow domain of fluid, imposing the boundary conditions similar to the realistic practical conditions and attaining the solution by solving the governing transport equations. The present research work is aimed at investigating the effect of heat flux on pressure drop and heat transfer by using computational fluid dynamics (CFD) approach. In order to solve governing fluid transport equations in CFD, finite volume method (FVM) is employed. The varying flow rates of 10 L/min to 30 L/min are considered at the inlet matching with experimental conditions and outflow boundary condition is employed at outlet to satisfy the continuity equation (1). Various heat loads acting on the surface of inner corrugated pipe are imposed as total heat flux on surface of computational domain as boundary condition. The constant thermo-physical properties of SCN at 129.19 K and 34 bar are considered for the present analysis as shown in Table 1 [14]. At various flow rates, conservation equations (Reynolds Averaged Navier-Stokes equations) such as fluid flow (mass, momentum), heat transfer (energy) and turbulence are solved simultaneously by CFD approach [18–20].

The time-averaged conservation of mass (continuity equation) for 3-D flow can be written as:

$$\frac{\partial \overline{u}}{\partial x} + \frac{\partial \overline{v}}{\partial y} + \frac{\partial \overline{w}}{\partial z} = 0 \tag{1}$$

where, u, v and w are known as time-averaged velocity components in x, y and z directions respectively. The time-averaged conservation of momentum equations for 3-D flow are as follows:

X-momentum

$$\rho \left(\frac{\partial \overline{u}}{\partial t} + \frac{\partial \overline{u}}{\partial x} + \frac{\partial \overline{u}}{\partial y} + \frac{\partial \overline{u}}{\partial y} + \frac{\partial \overline{u}}{\partial z} \right) = F_X - \frac{\partial \overline{p}}{\partial x} + \mu \nabla^2 \overline{u} - \rho \left(\frac{\partial \overline{u'u'}}{\partial x} + \frac{\partial \overline{u'v'}}{\partial y} + \frac{\partial \overline{u'w'}}{\partial z} \right)$$
(2)

Y-momentum

$$\rho \left(\frac{\partial \overline{v}}{\partial t} + \overline{u} \frac{\partial \overline{v}}{\partial x} + \overline{v} \frac{\partial \overline{v}}{\partial y} + \overline{w} \frac{\partial \overline{v}}{\partial z} \right) = F_{Y} - \frac{\partial \overline{p}}{\partial y} + \mu \nabla^{2} \overline{v} - \rho \left(\frac{\partial \overline{u'v'}}{\partial x} + \frac{\partial \overline{v'v'}}{\partial y} + \frac{\partial \overline{w'v'}}{\partial z} \right)$$
(3)

Z-momentum

$$\rho \left(\frac{\partial \overline{w}}{\partial t} + \overline{u} \frac{\partial \overline{w}}{\partial x} + \overline{v} \frac{\partial \overline{w}}{\partial y} + \overline{w} \frac{\partial \overline{w}}{\partial z} \right) = F_z - \frac{\partial \overline{p}}{\partial z} + \mu \nabla^2 \overline{w} - \rho \left(\frac{\partial \overline{u'w'}}{\partial x} + \frac{\partial \overline{v'w'}}{\partial y} + \frac{\partial \overline{w'w'}}{\partial z} \right)$$
(4)

where,
$$\nabla^2 \overline{u} = \left(\frac{\partial^2 \overline{u}}{\partial x^2} + \frac{\partial^2 \overline{u}}{\partial y^2} + \frac{\partial^2 \overline{u}}{\partial z^2}\right) \nabla^2 \overline{v} = \left(\frac{\partial^2 \overline{v}}{\partial x^2} + \frac{\partial^2 \overline{v}}{\partial y^2} + \frac{\partial^2 \overline{v}}{\partial z^2}\right) \nabla^2 \overline{w} = \left(\frac{\partial^2 \overline{w}}{\partial x^2} + \frac{\partial^2 \overline{w}}{\partial y^2} + \frac{\partial^2 \overline{w}}{\partial z^2}\right) \nabla^2 \overline{w} = \left(\frac{\partial^2 \overline{w}}{\partial x^2} + \frac{\partial^2 \overline{w}}{\partial y^2} + \frac{\partial^2 \overline{w}}{\partial z^2}\right) \nabla^2 \overline{w} = \left(\frac{\partial^2 \overline{w}}{\partial x^2} + \frac{\partial^2 \overline{w}}{\partial y^2} + \frac{\partial^2 \overline{w}}{\partial z^2}\right) \nabla^2 \overline{w} = \left(\frac{\partial^2 \overline{w}}{\partial x^2} + \frac{\partial^2 \overline{w}}{\partial y^2} + \frac{\partial^2 \overline{w}}{\partial z^2}\right) \nabla^2 \overline{w} = \left(\frac{\partial^2 \overline{w}}{\partial x^2} + \frac{\partial^2 \overline{w}}{\partial z^2} + \frac{\partial^2 \overline{w}}{\partial z^2} + \frac{\partial^2 \overline{w}}{\partial z^2}\right) \nabla^2 \overline{w} = \left(\frac{\partial^2 \overline{w}}{\partial x^2} + \frac{\partial^2 \overline{w}}{\partial z^2} + \frac{\partial^2 \overline{w}}{\partial z^2} + \frac{\partial^2 \overline{w}}{\partial z^2}\right) \nabla^2 \overline{w} = \left(\frac{\partial^2 \overline{w}}{\partial x^2} + \frac{\partial^2 \overline{w}}{\partial z^2} + \frac{\partial^2 \overline{w}}{\partial z^2} + \frac{\partial^2 \overline{w}}{\partial z^2}\right) \nabla^2 \overline{w} = \left(\frac{\partial^2 \overline{w}}{\partial x^2} + \frac{\partial^2 \overline{w}}{\partial z^2} + \frac{\partial^2 \overline{w}}{\partial z^2} + \frac{\partial^2 \overline{w}}{\partial z^2}\right) \nabla^2 \overline{w} = \left(\frac{\partial^2 \overline{w}}{\partial x^2} + \frac{\partial^2 \overline{w}}{\partial z^2} + \frac{\partial^2 \overline{w}}{\partial z^2} + \frac{\partial^2 \overline{w}}{\partial z^2}\right) \nabla^2 \overline{w} = \left(\frac{\partial^2 \overline{w}}{\partial x^2} + \frac{\partial^2 \overline{w}}{\partial z^2} + \frac{\partial^2 \overline{w}}{\partial z^2} + \frac{\partial^2 \overline{w}}{\partial z^2}\right) \nabla^2 \overline{w} = \left(\frac{\partial^2 \overline{w}}{\partial x^2} + \frac{\partial^2 \overline{w}}{\partial z^2} + \frac{\partial^2 \overline{w}}{\partial z^2} + \frac{\partial^2 \overline{w}}{\partial z^2}\right) \nabla^2 \overline{w} = \left(\frac{\partial^2 \overline{w}}{\partial x^2} + \frac{\partial^2 \overline{w}}{\partial z^2} + \frac{\partial^2 \overline{w}}{\partial z^2} + \frac{\partial^2 \overline{w}}{\partial z^2}\right) \nabla^2 \overline{w} = \left(\frac{\partial^2 \overline{w}}{\partial z^2} + \frac{\partial^2 \overline{w}}{\partial z^2} + \frac{\partial^2 \overline{w}}{\partial z^2} + \frac{\partial^2 \overline{w}}{\partial z^2}\right) \nabla^2 \overline{w} = \left(\frac{\partial^2 \overline{w}}{\partial z^2} + \frac{\partial^2 \overline{w}}{\partial z^2} + \frac{\partial^2 \overline{w}}{\partial z^2} + \frac{\partial^2 \overline{w}}{\partial z^2}\right) \nabla^2 \overline{w} = \left(\frac{\partial^2 \overline{w}}{\partial z^2} + \frac{\partial^2 \overline{w}}{\partial z^2} + \frac{\partial^2 \overline{w}}{\partial z^2} + \frac{\partial^2 \overline{w}}{\partial z^2}\right) \nabla^2 \overline{w} = \left(\frac{\partial^2 \overline{w}}{\partial z^2} + \frac{\partial^2 \overline{w}}{\partial z^2} + \frac{\partial^2 \overline{w}}{\partial z^2} + \frac{\partial^2 \overline{w}}{\partial z^2}\right) \nabla^2 \overline{w} = \left(\frac{\partial^2 \overline{w}}{\partial z^2} + \frac{\partial^2 \overline{w}}{\partial z^2} + \frac{\partial^2 \overline{w}}{\partial z^2} + \frac{\partial^2 \overline{w}}{\partial z^2}\right) \nabla^2 \overline{w} = \left(\frac{\partial^2 \overline{w}}{\partial z^2} + \frac{\partial^2 \overline{w}}{\partial z^2} + \frac{\partial^2 \overline{w}}{\partial z^2} + \frac{\partial^2 \overline{w}}{\partial z^2}\right) \nabla^2 \overline{w} = \left(\frac{\partial^2 \overline{w}}{\partial z^2} + \frac{\partial^2 \overline{w}}{\partial z^2} + \frac{\partial^2 \overline{w}}{\partial z^2}\right) \nabla^2 \overline{w} = \left(\frac{\partial^2 \overline{w}}{\partial z^2} + \frac{\partial^2 \overline{w}}{\partial z^2} + \frac{\partial^2 \overline{w}}{\partial z^2}\right) \nabla^2 \overline{w} = \left(\frac{\partial^2 \overline{w}}{\partial z^2} + \frac{\partial^2 \overline{w}}{\partial z^2}\right) \nabla^2 \overline{w} = \left(\frac{\partial$$

The generalized time-averaged momentum equation for all three directions in tensor form can be written as

$$\rho \frac{D\overline{u}_{i}}{Dt} = F_{i} - \frac{\partial \overline{p}}{\partial x_{i}} + \mu \nabla \overline{u}_{i} - \rho \left(\frac{\partial u_{i} u_{j}}{\partial x_{j}} \right)$$

$$(5)$$

i and j are the normal components of tensor taking a value of Zero if i≠j and One if i=j,

 $\rho \left(\frac{\partial \overrightarrow{u_i u_j}}{\partial x_j} \right)_{\text{is characterized as}}$

Reynolds stress or turbulent shear stress and $\left(\mu \frac{\partial u_i}{\partial x_j} - \rho \overrightarrow{u_i u_j}\right)$ is known as total shear stress τ_{ij} . u represent the

instantaneous velocity component, and u' is known as fluctuating velocity component. F_x , F_y and F_z are known as body forces and neglected for the present simulations.

The time-averaged energy equation for 3-D flow are as follows:

$$\rho C_{p} \left[\overline{u} \frac{\partial \overline{T}}{\partial x} + \overline{v} \frac{\partial \overline{T}}{\partial y} + \overline{v} \frac{\partial \overline{T}}{\partial z} \right] = \frac{\partial}{\partial x} \left[k \frac{\partial T}{\partial x} - \rho C_{p} \overline{u'T'} \right] + \frac{\partial}{\partial y} \left[k \frac{\partial T}{\partial y} - \rho C_{p} \overline{v'T'} \right] + \frac{\partial}{\partial z} \left[k \frac{\partial T}{\partial z} - \rho C_{p} \overline{w'T'} \right]$$
(6)

The steady, incompressible flow of SCN are solved computationally using the time averaged Reynolds Average Navier-Stokes (RANS) equations. The governing equations that are discussed in this section are solved using the Finite Volume Method (FVM) of discretization and $\kappa - \varepsilon$ turbulence scheme as a closure to RANS equations. To obtain the accurate results, temperature dependent thermophysical properties of SCN are used during the analysis. The ANSYS-FLUENT [18] is used to solve the computational model with imposed boundary conditions.

The wall shear stresses that are developed due to the turbulent flow of SCN in HTS cable is used for calculating the friction factors at different flow rates and heat loads using equation (7) as

$$f = \frac{8\tau_{wall}}{\rho v_{avg}^2} \tag{7}$$

where, τ_{wall} is shear stress developed at the wall of the former (Pa), v_{avg} is average velocity of SCN (m/s). The Reynolds number for different flow rates of temperature dependent SCN flow in the HTS cable can be calculated using equation (8) as

$$Re = \frac{\rho_{SCN} v_{avg} D_h}{\mu_{SCN}}$$
 (8)

where, D_h is the hydraulic diameter of the computational domain (m), μ_{SCN} is viscosity of SCN (Pa-s). The pressure drop in the computational domain is due to the turbulent friction flow of SCN in HTS cables and can be estimated using equation (9) as

$$\Delta p = \left(\frac{\text{Re}\,\mu_{SCN}}{D_h}\right) \left(\frac{fLv_{avg}}{2D_h}\right) \tag{9}$$

The power required to circulate the SCN through the corrugated former HTS cable can be calculated using equation (10) as

$$W = \Delta p \stackrel{\sqcup}{V} \tag{10}$$

where, Δp is pressure drop (Pa), L is length of HTS cable (m), v_{avg} is average velocity (m/s) and ρ_{SCN} is density

(kg/m³) of SCN, $V = A_c \cdot v_{avg}$ is volumetric flow rate of the SCN and A_c is the cross sectional area of (m²) respectively.

RESULTS AND DISCUSSION

The present work is focused on investigating the effect of various heat loads on pressure drop and heat transfer of SCN flowing through inner corrugated steel pipe in the HTS cable as shown in figure 1. In this section, the results of pressure drop in inner corrugated steel pipe and heat transfer from corrugated pipe to SCN are presented. Pressure drop is generally described as the difference in total pressure between any two sections of a fluid carrying channel. Frictional forces, caused by the resistance to flow, generates pressure drop in a fluid stream flowing through the channel.

Pressure drop rises proportional to the frictional shear forces produced by corrugated pipe within the HTS cable. Moreover, surface roughness and corrugations of corrugated pipe within the HTS cable will affect the pressure drop. In addition, the key factors resulting in a larger pressure drop across the corrugated pipe are high flow velocities and fluid viscosity. The computational estimation of pressure drop per unit length (Pa/m) for the present work is first compared with the available published results from simulation and experimentation by Li et al. [19]. Also, the 3-D HTS cable model is designed with same diameter of 40 mm and pitch of 6 mm as Li et al. [19] for the validation. The obtained pressure drop for the present work (SCN as coolant) is found to be lesser than annulus corrugated flow (LN2 as coolant) as shown in Figure 3. Lower pressure drop in the present work occurs due to the lower fluid viscosity and density of SCN than that of LN2. Moreover, the effect of various heat loads on friction factor with Reynolds number ranging from 60,000 to 210000 is shown in Figure 4 (a). It is observed from the results that friction factor for the present analysis is independent of the heat loads and decreases with higher flow rates. The pumping power with volumetric flow rate at various heat loads for SCN flowing through inner corrugated pipe can be seen in Figure 4 (b). It is observed from the results that pumping power rises with increase in the flow rates and independent of heat loads.

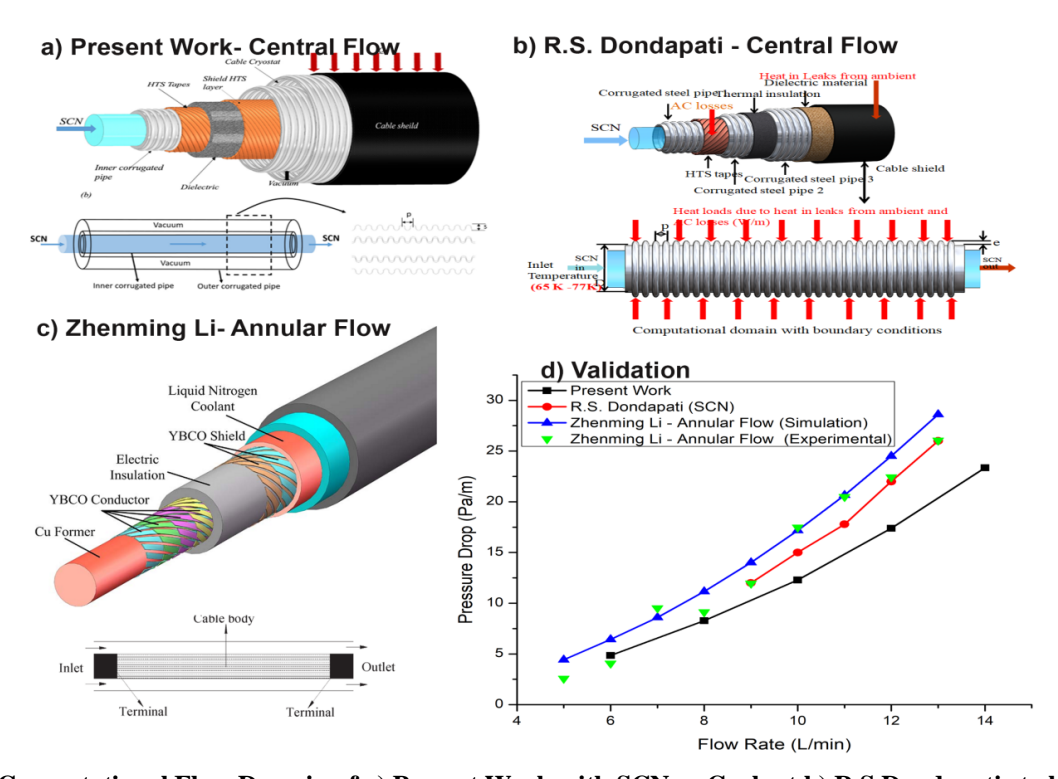


Figure 3. Computational Flow Domain of a) Present Work with SCN as Coolant b) R.S.Dondapati et al with SCN as coolant [20] c) Zhenming Li et al., with LN2 as coolant [19] d) Validation of attained pressure drop for SCN with simulation and experimental results performed for LN2 and SCN

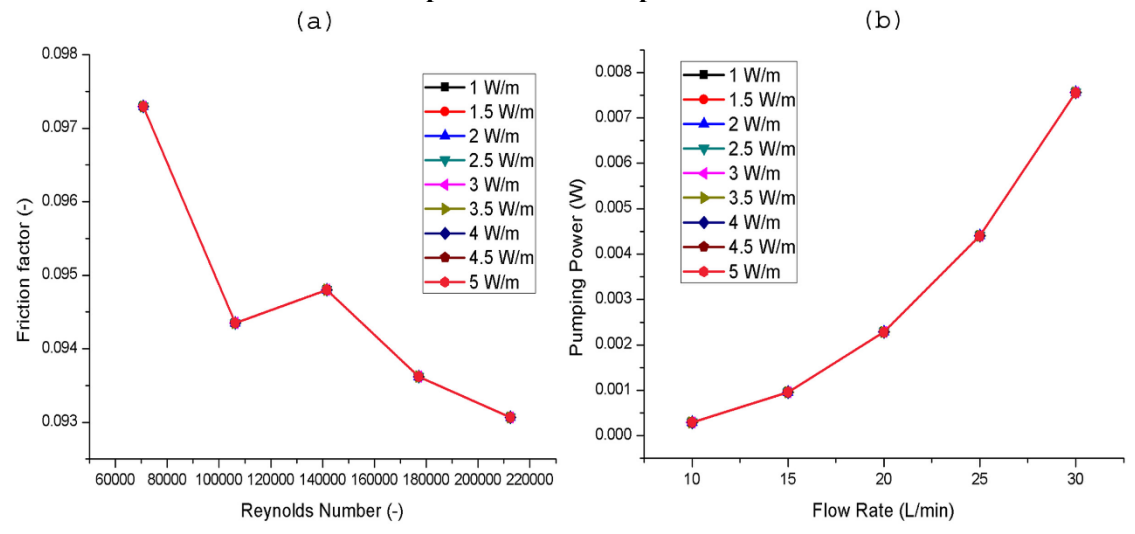


Figure 4. Effect of heat loads on (a) friction factor (b) pumping power

In this section, various parameters such as temperature difference and cooling capacity are estimated in order to predict the effect of heat flux on heat transfer rate between SCN and corrugated pipe wall. The inlet and outlet temperatures are also estimated for SCN. Moreover, the estimated temperature difference for SCN at a heat load of 2.1 W/m are validated with the results of liquid nitrogen available in the literature as shown in Figure 5. The lower temperature difference for SCN is observed than that with LN2. In addition, the heat transfer analysis of SCN in terms of cooling capacity is also represented in Figure 6(a). It can be observed from the results that with increase in the flow rates, the required cooling capacity of HTS cable system with SCN increases first and remains constant. The effect of higher flow rates on required cooling capacity is insignificant. Moreover, the required cooling capacity is found to be approximately 12 W at total heat load of 5 W/m. Figure 6 (b) depicts the temperature difference at various total heat loads (A.C loss, Dielectric loss and heat-in-leak) as a function of flow rates of SCN through inner corrugated pipe. It can be perceived that the temperature difference between outlet and inlet increases as the heat load increases for a particular flow rate which results in removing of heat accommodated in the HTS cable.

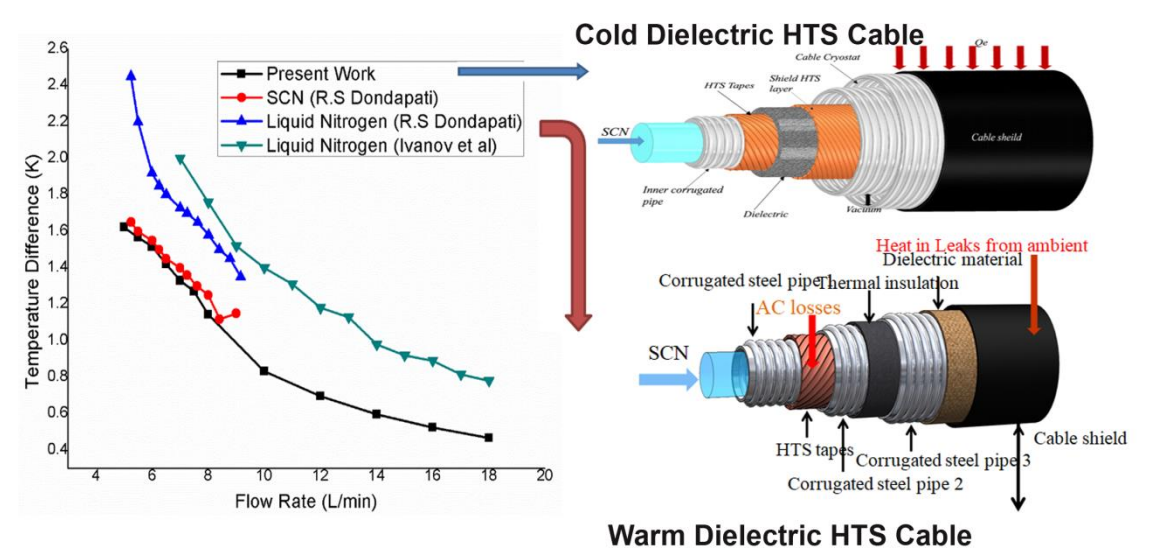


Figure 5. Comparison between the results of Cold Dielectric and Warm Dilectric HTS Cables [21] and [20]

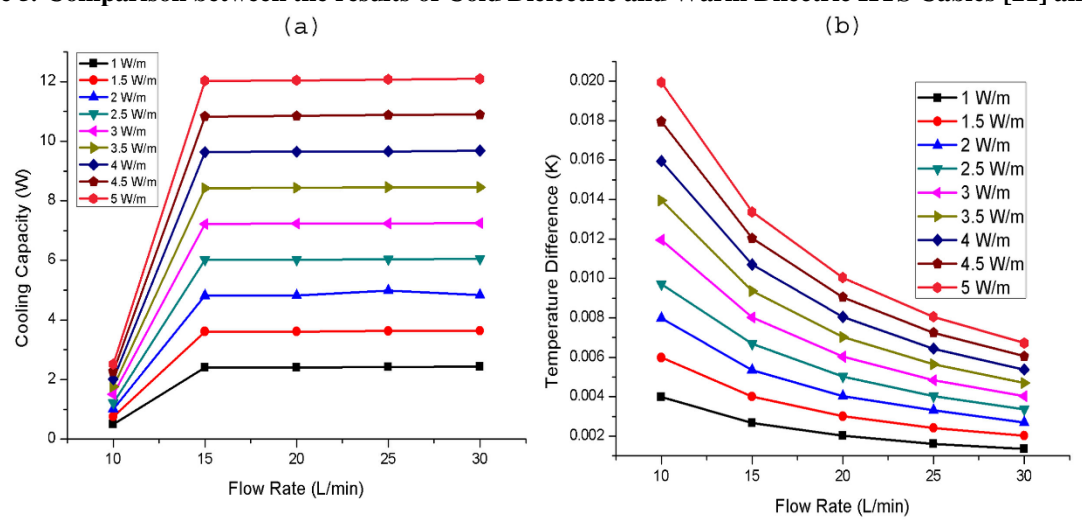


Figure 6. (a) Cooling capacity of SCN at various heat loads (b) Temperature difference of SCN between inlet and oulet points at various heat loads

CONCLUSIONS

In the present work, Super Critical Nitrogen (SCN) was proposed as an alternative coolant for futuristic HTS tapes such as Hg based of critical temperature greater than 134 K. Moreover, the effect of different heat flux on pressure drop and heat transfer with SCN in futuristic cold dielectric HTS cables has been carried out using CFD. The obtained pressure drop and heat transfer results of SCN are then compared with LN2 experimental and SCN computational results available in the literature. The obtained pressure drop for the present work (SCN as coolant) is found to be lesser than annulus corrugated flow (LN2 as coolant) and other corrugated inflow (SCN as coolant). Therefore, the lesser pressure drop in the HTS cable results the lesser pumping power to pump SCN through inner corrugated pipe due to lower density and viscosity. In addition, the minimum pumping power required to pump the SCN across corrugated pipe is observed as 0.008W for 0.504 m length of HTS cable at flow rate of 30 L/min. Moreover, the temperature difference of inlet and outlet for SCN are estimated and validated with liquid nitrogen and SCN results available in the literature. The

obtained temperature difference for SCN is also found to be lesser than that of LN2. Furthermore, cooling capacity can also be improved using SCN due to its higher specific heat as compared of LN2. Hence, SCN may be considered as one of the alternative solutions for cooling of futuristic Hg-based cold dielectric HTS cables. It is also essential to study the effect of stress generated due to the higher pressure of SCN on the corrugated pipe.

REFERENCES

- [1] G. Vyas and R. S. Dondapati, "AC losses in the development of superconducting magnetic energy storage devices," *J. Energy Storage*, vol. 27, p. 101073, 2020.
- [2] R. S. Dondapati, "Investigation on the degradation of thermohydraulic performance of high temperature superconducting (HTS) cables used for large scale energy storage and transmission applications caused by entropy generation," *Phys. C Supercond. its Appl.*, vol. 600, p. 1354102, 2022.
- [3] R. S. Dondapati, High-Temperature Superconducting Devices for Energy Applications. CRC Press, 2020.
- [4] R. S. Dondapati and V. V Rao, "Long Length Internally Cooled HTS Cables," vol. 23, no. 3, pp. 2–5, 2013.
- [5] R. S. Dondapati, J. Ravula, S. Thadela, and P. R. Usurumarti, "Analytical approximations for thermophysical properties of supercritical nitrogen (SCN) to be used in futuristic high temperature superconducting (HTS) cables," *Phys. C Supercond. its Appl.*, vol. 519, pp. 53–59, 2015.
- [6] M. Kalsia, R. S. Dondapati, and P. R. Usurumarti, "Statistical correlations for thermophysical properties of Supercritical Argon (SCAR) used in cooling of futuristic High Temperature Superconducting (HTS) cables," *Phys. C Supercond. its Appl.*, vol. 536, pp. 30–34, 2017.
- [7] J. A. Demko *et al.*, "Testing of a 1 . 5-m Single-Phase Short-Sample Cable Made With Copper Laminated HTS Tapes at ORNL," vol. 15, no. 2, pp. 1755–1758, 2005.
- [8] R. Martin, "CRYOGENIC SYSTEM FOR A HIGH-TEMPERATURE TRANSMISSION CABLE *."
- [9] L. H. T. S. Cables, J. A. Demko, and R. C. Duckworth, "Cooling Configuration Design Considerations for," vol. 19, no. 3, pp. 1752–1755, 2009.
- [10] J. Bin Song and H. Lee, "Mixed cryogen cooling systems for HTS power applications: A status report of progress in Korea University," *Cryogenics (Guildf).*, vol. 52, no. 12, pp. 648–655, 2012.
- [11] D. Kim, H. Park, S. Kim, H. Jang, and Y. Kim, "Dynamic Characteristics of Pressure Build Up Tank for HTS Power Cable Refrigeration System," *Phys. Procedia*, vol. 58, pp. 334–337, 2014.
- [12] O. Maruyama, T. Ohkuma, and T. Izumi, "Numerical analysis of heat transfer and fluid characteristics in long distance HTS cable," *Phys. Procedia*, vol. 45, pp. 285–288, 2013.
- [13] H. M. Chang and S. I. Lee, "Conduction-Cooling System for Superconducting Magnets at 20-30 K," *IEEE Trans. Appl. Supercond.*, vol. 24, no. 3, pp. 3–6, 2014.
- [14] E. W. Lemmon, M. L. Huber, and M. O. Mclinden, "NIST Reference Fluid Thermodynamic and Transport Properties REFPROP," National Institute of Standards and Technology, Boulder, Colorado (USA), 2010.
- [15] M. Kalsia and R. S. Dondapati, "Influence of flow rate and heat flux on the temperature distribution in long length counter flow cooled cold dielectric HTS cables," *Phys. C Supercond. its Appl.*, vol. 567, p. 1353549, 2019.
- [16] M. Kalsia and R. S. Dondapati, "Thermohydraulic analysis of cold dielectric high temperature superconducting cable with counter-flow cooling," *Phys. C Supercond. its Appl.*, vol. 564, pp. 59–67, 2019.
- [17] M. Kalsia and R. S. Dondapati, "Influence of corrugation topology on thermohydraulic performance of cold dielectric counter cooled high temperature superconducting cable," *Phys. C Supercond. its Appl.*, vol. 566, p. 1353525, Jun. 2019.
- [18] ANSYS-Fluent Theory Guide. Canonsburg, PA: Ansys Inc, 2013.
- [19] Z. Li, Y. Li, W. Liu, J. Zhu, and M. Qiu, "Comparison of Liquid Nitrogen Flow Resistance in Corrugated Pipe With Smooth Pipe for HTS Cable," *IEEE Trans. Appl. Supercond.*, vol. 25, no. 3, p. 5401304, 2015.
- [20] R. Sekhar Dondapati, "Role of Supercritical Nitrogen (SCN) on the Hydraulic and Thermal characteristics of futuristic High Temperature Superconducting (HTS) Cables," *Cryogenics (Guildf).*, p. 103166, 2020.
- [21] Y. V Ivanov, H. Watanabe, M. Hamabe, J. Sun, T. Kawahara, and S. Yamaguchi, "Circulation pump power for 200 m cable experiment," *Phys. C Supercond. its Appl.*, vol. 471, no. 21–22, pp. 1308–1312, 2011.